Frequency-Dependent Connectivity in Large-Scale Resting-State Brain Networks during Sleep

Simon Titone [1,2], Jessica Samogin [1], Philippe Peigneux [3], Stephan P. Swinnen [1,2], Dante Mantini [1], Genevieve Albouy [1,2,4]*

[1] Department of Movement Sciences, Movement Control and Neuroplasticity Research Group, KU Leuven, Leuven, Belgium

[2] LBI – KU Leuven Brain Institute, KU Leuven, Leuven, Belgium

[3] Neuropsychology and Functional Neuroimaging Research Group (UR2NF) at the Centre for Research in Cognition and Neurosciences (CRCN), Université Libre de Bruxelles (ULB), Brussels, Belgium

[4] Department of Health and Kinesiology, College of Health, University of Utah, Utah, USA

* Correspondence: GA: Genevieve.albouy@kuleuven.be

Abstract:

Functional connectivity (FC) during sleep has been shown to break down as non-rapid eye movement (NREM) sleep deepens before returning to a state closer to wakefulness during REM sleep. However, the specific spatial and temporal signatures of these fluctuations in connectivity patterns remain poorly understood. The goal of this study was to investigate how frequency-dependent network-level FC fluctuates during nocturnal sleep in healthy young adults using high-density electroencephalography (hdEEG). Specifically, we examined source-localized FC in resting-state networks during NREM2, NREM3, and REM sleep in the first three sleep cycles of 29 participants. Our results showed that FC within and between all resting-state networks decreased from NREM2 to NREM3 sleep in multiple frequency bands and in all sleep cycles. The data also highlighted a complex modulation of connectivity patterns during the transition to REM sleep whereby delta and sigma bands hosted a persistence of the connectivity breakdown in all networks, whereas a reconnection was observed in the default mode (DMN) and the attentional networks in frequency bands characterizing their organization during wake (i.e., alpha and beta bands, respectively). Finally, all network pairs (except the visual network) showed higher gamma-band FC during REM sleep in cycle three compared to earlier cycles during the night. Altogether, our results unravel the spatial and temporal characteristics of the well-known breakdown in connectivity observed as NREM sleep deepens. They also shed light on a complex pattern of connectivity during REM sleep that is consistent with both breakdown and reconnection processes that are network- and frequency-specific.

Introduction:

Functional connectivity (FC) is a measure that reflects the relationship between neural signals over time (Waites *et al.*, 2005; Wens *et al.*, 2014; Nikolaou *et al.*, 2016; Gaudet *et al.*, 2020). FC studies have shown that brain responses are organized in networks of co-activation that are related to specific functions (e.g., attentional, motor, visual functions, etc.; Biswal et al., 1995; Raichle et al., 2001; Fox et al., 2006). These function-specific networks can also be identified during a state of relative inactivity referred to as "resting-state" (Biswal *et al.*, 1997; Greicius *et al.*, 2003) and display common neural substrates across multiple neuroimaging modalities such as functional magnetic resonance imaging (fMRI; Raichle et al., 2001), magnetoencephalography (MEG; de Pasquale et al., 2010), high-density electroencephalography (hdEEG; Samogin et al., 2019) and positron emission tomography (PET; Savio et al., 2017). Recent research has demonstrated that brain responses during sleep are also organized into functional large-scale brain networks that correspond to the well-known canonical resting-state networks (Houldin *et al.*, 2019). While there is evidence that resting-state network topology is preserved during sleep, the modulation of connectivity patterns associated with the extensive changes in brain oscillatory activity and synchrony that occur across stages and cycles of sleep are not yet fully understood.

The descent into sleep is behaviorally marked by decreased engagement with external stimuli and a loss of consciousness. Previous research has demonstrated that FC patterns observed during wakefulness are generally maintained during non-rapid-eye-movements sleep stage 1 (NREM1) in sensory (i.e., auditory, somatomotor, and visual) and cognitive (dorsal attention, default, and executive control) networks, while moderate increases in connectivity are reported within the dorsal attention network (Larson-Prior *et al.*, 2009). FC during deeper NREM sleep is described to become more dissimilar to wake as sleep progressively deepens into NREM2 and NREM3 (Houldin *et al.*, 2021). Specifically, the transition to NREM sleep is characterized by decreases in large-scale functional connectivity. Seminal work from Massimini and collaborators (Massimini *et al.*, 2005) revealed that transcranial magnetic stimulation (TMS)-induced propagation of activity across brain regions decreased during NREM2-3 sleep compared to wake, suggesting a breakdown of effective cortical connectivity during these sleep stages. Considerable data now supports the idea that long-range connectivity decreases during NREM3 sleep (for review, see Spoormaker et al., 2010). Neuroimaging research also indicates that across multiple networks (e.g., motor, visual, default mode network DMN), connectivity is functionally clustered into smaller independent modules during NREM sleep, such that within-system integration becomes higher than between-system integration (Boly *et al.*, 2012). Nonetheless, total brain integration (the sum of information exchanged within and between major large-scale networks) is increased during NREM sleep compared to wake (Boly *et al.*, 2012). During REM sleep, cortical connectivity appears to return to a state closer to wakefulness, with communication occurring in a more

widespread manner (Massimini *et al.*, 2010). For example, connectivity in frontoparietal and somatosensory networks has been described to increase during REM as compared to NREM sleep (Watanabe *et al.*, 2014). Results regarding DMN connectivity during REM sleep are less consistent as previous research reported no changes (core DMN; Koike et al., 2011), increases (sub-components of DMN; Koike et al., 2011) or even decreases in DMN FC (Watanabe *et al.*, 2014). In sum, the evidence reviewed above indicates that overall long-range functional connectivity decreases during the descent into NREM sleep. The pattern of results is less consistent during REM sleep, but a general trend for a return to wake-like state connectivity patterns has been reported in specific networks.

The above-mentioned research mainly used neuroimaging techniques such as fMRI and PET to investigate resting-state functional connectivity during sleep. While these methods are advantageous due to their excellent spatial accuracy, they are unable to distinguish frequency-dependent characteristics of connectivity patterns. Investigating the spectral signatures of brain connectivity within and between large-scale networks is particularly relevant during sleep, as this vigilance state is characterized by circuit-specific oscillations (Adamantidis *et al.*, 2019). For example, early research using graph theory has shown frequency-specific changes in electroencephalography (EEG) connectivity during sleep, such that overall connectivity increased from wake to sleep in the alpha, sigma, and beta frequency bands while a decrease was observed in the theta band (Ferri *et al.*, 2007, 2008). Finer-grained analyses of stage-specific effects demonstrated that global field synchronization (GFS) was higher in the sigma frequency band during NREM sleep compared to other sleep stages, whereas synchronization was greater in all bands excluding the theta and sigma bands during REM as compared to NREM2-3 sleep (Achermann *et al.*, 2016). Additionally, recent work using EEG coherence analysis performed at the channel level has revealed that connectivity in the delta and theta bands was greater during NREM2 as compared to NREM3, while delta connectivity shows a general decrease during the transition from NREM to REM (Bouchard *et al.*, 2019). Interestingly, delta-connectivity was described to stay consistent across cycles of NREM2 sleep and increase across cycles of NREM3 (Bouchard *et al.*, 2019). Overall, these studies suggest that connectivity is particularly elevated in the delta, sigma, and theta bands during NREM sleep and in the alpha, beta, and gamma bands during REM sleep. While these electrophysiological studies indicate frequency-dependent fluctuations of FC during sleep, they did not examine connectivity in the functionally organized (and spatially specific) networks described above. Thus, a comprehensive characterization of frequency-dependent changes in connectivity in functional resting-state networks is currently lacking.

The goal of our study was, therefore, to examine how frequency-dependent network-level FC fluctuates as an effect of stages (NREM2, NREM3, and REM) and cycles (first, second, and third cycles) of nocturnal sleep in young, healthy individuals. To do so, we used high-density electroencephalography (hdEEG) and recent advances in computational techniques

to measure frequency-dependent FC in source-localized resting-state networks (Liu *et al.*, 2017; Samogin *et al.*, 2020; Titone *et al.*, 2022). EEG connectivity measures were obtained by computing correlations between power time courses from seeds of interest. Connectivity within and between six resting-state networks defined from previous fMRI literature (de Pasquale *et al.*, 2012) was then examined. Based on previous literature, we predicted that connectivity would globally decrease between large-scale brain networks as NREM sleep deepens, while within-network connectivity was expected to increase (Boly *et al.*, 2012; Houldin *et al.*, 2021). We hypothesized that this modulation would be particularly prominent in the delta, theta, and sigma frequency bands (Bouchard et al., 2019; Achermann et al., 2016). During REM sleep, connectivity was expected to increase as compared to NREM, especially within the sensorimotor, attentional, and default mode networks (Wu *et al.*, 2012; Watanabe *et al.*, 2014; Houldin *et al.*, 2021). At the frequency level, we hypothesized that connectivity in the alpha, beta, and gamma frequency bands would be greater in REM than in NREM sleep (Achermann *et al.*, 2016; Bouchard *et al.*, 2019). With respect to changes across sleep *cycles*, we predicted that large-scale NREM2 FC would not change significantly across *cycles* in all frequency bands and that NREM3 FC would show a general cross-cycle increase in the delta band across networks (Bouchard *et al.*, 2019). Earlier research has never examined network dynamics during REM sleep across sleep cycles, but we anticipated a global increase in alpha, beta, and gamma connectivity (Achermann *et al.*, 2016) across sleep cycles.

Methods:

Participants

Twenty-nine young (23.7 ± 3.3 years old, 15 females) right-handed (Oldfield, 1971) healthy volunteers were recruited to complete this study. Participants reported no history of medical, neurological, or psychiatric disorders. They also showed no evidence of anxiety (Beck *et al.*, 1988), depression (Beck, 1961), or excessive daytime sleepiness (Johns, 1991). Participants had normal sleep quality as assessed by the Pittsburg Sleep Quality Index questionnaire (Buysse *et al.*, 1989) and the Saint Mary's Hospital questionnaire (Ellis *et al.*, 1981). None of the participants were extreme morning or evening chronotypes (Horne & Ostberg, 1976) or shift workers, nor did any report trans-meridian trips in the three months before the experiment.

Out of the 29 participants who took part in the study, two participants were excluded for not respecting a constant sleep schedule before the experiment. An additional participant was excluded as they presented a high number of respiratory events during the habituation night. The remaining 26 participants (23.7 ± 3.5 years old, 14 females; see Supplemental table 1 for participant demographics) were included in the analyses. Further participant exclusion was based on the outcome of the EEG data analysis and included (i) the absence of five consecutive minutes of sleep in the studied sleep stage and cycle and (ii) showing outlier connectivity metrics (mean ± 3*standard deviation) across multiple frequency bands and network pairs. The resulting sample sizes are reported in the results section for each analysis and in Supplemental Table 2.

Experimental procedure

The research presented in this manuscript is part of a larger experimental protocol completed by the same cohort of participants (see Supplemental Figure 1 for the full design). One to four weeks preceding the experimental session, participants came to the sleep lab for a habituation session during which they were introduced to the general study procedure and slept overnight with the hdEEG cap on (habituation night; Figure 1). To assess possible sleep disorders, they wore additional electrodes on the legs, along with a respiratory belt and thermistor to measure breathing. Participants were asked to keep a constant sleep schedule and refrain from drinking alcohol and taking naps for the four days preceding the experimental session. Compliance with this schedule was assessed using sleep diaries and wrist actigraphy (ActiGraph wGT3X-BT, Pensacola, FL). During the experimental session, participants spent approximately 10 hours in the lab from 8-10 pm to 7-9 am the next morning. After the hdEEG cap was set up, participants were allowed to read or watch TV until they felt ready to sleep (bedtime between 10:45 pm-00:15 am). Before lights were turned off, a 3D scan

of the electrode positions was completed (see details below). Participants woke up the next morning between 06:30[1]– 08:30, and the hdEEG cap was removed.

Neuroimaging data acquisition

EEG data acquisition

Brain activity during the habituation and experimental nights was recorded using 128-channel hdEEG ActiCHamp and BrainAmp amplifiers from BrainProducts (actiCHamp and BrainAmp, Brain Products GmbH, Gilching, Germany) at a sampling rate of 1000 Hz. Electrode FCz was used as a recording reference. The bilateral horizontal and vertical electrooculogram (EOG), along with chin and trapezius electromyogram (EMG), were recorded simultaneously with EEG recordings. Positions of EEG sensors were recorded using a structure sensor camera and Skanect 3D software from Occipital Inc. (Boulder, CO, USA) and localized using the SPOT3D toolbox (Taberna *et al.*, 2019).

MRI data acquisition

An anatomical T1-weighted 3D MP-RAGE sequence (TR=9.5 ms, TE=4.6 ms, TI=858.1 ms, FA=9◦, 160 slices, FoV=250×250 mm2, matrix size=256×256×160, voxel size=0.98×0.98×1.20 mm3) was acquired using a Phillips Achieva 3.0 T MRI System with a 32-channel head coil. RS fMRI scans were also acquired, but the corresponding data are not reported in the present manuscript.

Neurophysiological data analysis

Sleep scoring

Sleep was scored using an automated algorithm (Patanaik *et al.*, 2018) that uses two EEG (C3 and C4 referenced to the mastoid) and EOG (left and right EOG referenced to the mastoid) channels. The two EEG channels were averaged and band-pass filtered between 0.3 - 45 Hz, and the two EOG channels were filtered between 0.3 - 12 Hz. Data were then downsampled to 100 Hz and divided into 30s epochs. Short-time Fourier transform with a Hamming window length of 128 samples was then performed. A sixteen-layer deep convolutional neural network used the resulting spectrogram to assign a class probability to each epoch, with the sleep stage having the highest probability being considered the most probable class (MPC). A multilayer perceptron then weighed the MPC outputs to generate a revised class probability for the stage of the epoch, and the MPC was again calculated from that revised score. The automated sleep scores were visually checked epoch by epoch by an experimenter (ST). In case of a mismatch between the experimenter's and the algorithm's score, the experimenter's score was retained for the epoch.

[1] Note that one participant naturally woke up at 5:00am - thus before the earliest lights on time (6:30am). Importantly, this participant presented 6.5h of sleep and three sleep cycles and was therefore included in the analyses.

hdEEG resting-state functional connectivity analyses

Frequency-dependent functional connectivity was derived from the sleep EEG data with an automated workflow developed and validated by our team (Samogin *et al.*, 2019, 2020).

EEG signal preprocessing

EEG data were segmented into epochs consisting of the first five consecutive minutes available of each sleep stage of interest (i.e., NREM2, NREM3, and REM) in the first three sleep cycles (cycles one, two, and three) of the night. The start of cycle one was defined as the onset of the first period of NREM2 sleep that lasted longer than five minutes. The end of each sleep cycle – as well as the start of sleep cycles two and three - were marked by the end of a REM sleep period that lasted at least 30 seconds (Březinová, 1974; De Gennaro *et al.*, 2000; Le Bon *et al.*, 2019). This resulted in a maximum of 9 epochs per participant (but see participant exclusion as not all participants presented sufficient sleep data to extract nine epochs; e.g., the likelihood of five consecutive minutes of NREM3 in cycle three is lower than in earlier cycles).

The preprocessing of the EEG segments described above included the attenuation of noise and biological artifacts (Liu *et al.*, 2017; Samogin *et al.*, 2019). Channels with low quality were labeled as "bad channels" using the procedures from (Samogin *et al.*, 2020). The signal of each bad channel was then reconstructed from spatial interpolation of the neighboring channels, defined using the FieldTrip toolbox (http://www.fieldtriptoolbox.org). The resulting EEG data was band-pass filtered (1-80 Hz) using EEGLab (https://sccn.ucsd.edu/eeglab) and re-referenced to an average reference by removing the mean value across channels (Liu *et al.*, 2015). Independent component analysis (ICA) was used to attenuate muscular and ocular artifacts in EEG signals (Mantini *et al.*, 2008). Independent components were automatically identified using the artifact detection solution implemented by (Liu *et al.*, 2017). Non-artifactual ICs were mixed linearly with the ICA-estimated weights to obtain the artifact-corrected EEG signals (Samogin *et al.*, 2020).

Individual head model creation

T1 anatomical MR images were segmented into 12 different tissue classes. A realistic head model was then constructed from the segmented T1 and EEG sensor positions, which were rigidly co-registered to the contour of the head (Liu *et al.*, 2017; Samogin *et al.*, 2019). To define all possible dipole moments, a regular 3D 6mm grid was overlapped on all layers corresponding to cortical, subcortical, and cerebellar grey matter. Conductivity values were defined based on previous literature (Haueisen *et al.*, 1997). Next, SimBio (Wolters *et al.*, 2004; Ziegler *et al.*, 2014) was used to generate the whole-head finite element head model. Lastly, the head model was used to calculate a leadfield matrix expressing the linear relationship between scalp EEG data and source-space neural activity.

EEG source reconstruction

The exact low-resolution brain electromagnetic tomography (eLORETA) algorithm was used to compute the cortical 3-D distribution of current density derived from processed scalp EEG data (Pascual-Marqui *et al.*, 2011). The algorithm used the leadfield matrix as input to estimate source-space neural activity in a 6 mm homogenous grid constrained to the grey matter.

Network connectivity analyses

This research examined connectivity within and between six resting-state networks (RSNs) that have been commonly investigated in other studies. These networks cover a large portion of the cortical surface and include the default mode network (DMN), dorsal attention network (DAN), ventral attention network (VAN), somatomotor network (MOT), visual network (VIS), and language network (LANG). The nodes of these RSNs are based on previous literature (Mantini *et al.*, 2007; de Pasquale *et al.*, 2012; Grootswagers *et al.*, 2018; Samogin *et al.*, 2019) and have a minimum distance of 15mm between them to minimize spurious effects of signal leakage (see Supplemental Table 3 for coordinates). A 6mm sphere was defined around each MNI coordinate. For each resulting spherical ROI, a short-time Fourier transform was used to decompose the time courses of grey-matter voxels in the time-frequency domain. Then EEG connectivity was calculated using power envelope correlations between orthogonalized signals (Hipp *et al.*, 2012). Specifically, Pearson correlations were computed between ROIs per frequency band (range: 1–80 Hz) on the logarithmic-transformed signal-orthogonalized power time courses. The resulting r-values were transformed into z-scores using Fisher's transform (de Pasquale *et al.*, 2012; Hipp *et al.*, 2012). Z-scores were then averaged within relevant frequencies to calculate frequency band connectivity values between specific ROIs for the delta (1–4 Hz), theta (4–8 Hz), alpha (8–12 Hz), sigma (12–16 Hz), beta (16–30 Hz), and gamma (30–80 Hz) bands.

RSN connectivity was examined both within and between large-scale cortical networks. Connectivity within networks was computed by averaging connectivity between pairs of ROIs within each network, whereas between-network connectivity was calculated as the averaged connectivity between all possible pairs of ROIs from two distinct networks. This produced a 6 x 6 (network x network) connectivity matrix for each participant in each frequency band (6), sleep stage (3), and sleep cycle (3).

Statistical analyses were performed in Matlab 2016b (Mathworks; Natick, MA) on the within- and between-network connectivity values separately for the six frequency bands described above. Changes in connectivity between sleep *stages* and between sleep *cycles* were assessed with separate ANOVAs. For *inter-stage* connectivity analyses, separate repeated-measures ANOVAs were performed for each frequency band (delta, theta, alpha, sigma, beta, and gamma) and each sleep cycle (i.e., one, two, and three) using sleep stage (three levels: NREM2, NREM3, and REM) as within-subject factor. Follow-up pairwise comparisons were

performed for each significant effect. For *inter-cycle* connectivity analyses, separate repeated-measures ANOVAs were performed for each frequency band (delta, theta, alpha, sigma, beta, and gamma) and each sleep stage (i.e., NREM2, NREM3, and REM) using sleep cycle (three levels: one, two, and three) as within-subject factor. Note that statistical models including both sleep *stages* and *cycles* as within-subject factors resulted in low sample sizes and were therefore not included in the manuscript. For each of these analyses described above, the false discovery rate (FDR) method (Benjamini & Hochberg, 1995) was used to correct for multiple comparisons across all network pairs (21 in total). Results from the ANOVAs that survived FDR correction are reported in the main text, and follow-up pairwise tests are shown in the supplemental results (Section *Functional Connectivity: Follow-up Paired Comparisons*). ANOVAs showing significant uncorrected results are also reported in the supplemental results (Section *Functional Connectivity, Significant Uncorrected Results*).

Results:

Sleep quantity before and during the experimental night

Actigraphy and sleep diary data collected during the four nights preceding the experimental session indicated that participants slept on average more than 8 hours per night before the experiment (mean sleep duration across the four nights: 8 h 18 min ± 42 min; see details in Supplemental Table 4). A repeated-measures ANOVA using nights (4) as a within-subject factor indicated that sleep duration did not differ across the four nights preceding the experimental session ($F_{(3,60)} = 0.11$, $p = 0.96$). During the overnight sleep recording in the lab, the average total sleep time was 7 h 17 min ± 53 min, and sleep efficiency was 94.7% ± 3.9% (see Table 1 for sleep characteristics of the experimental night).

Table 1: Sleep characteristics from the overnight experimental EEG session (six participants are excluded from the sleep architecture data analyses due to amplifiers running out of battery before the end of the night; n = 20).

Experimental Night	
Time in bed (TIB) mins:	470.5 ± 31.4
Total sleep time (TST) mins:	441.8 ± 41.4
Wake after sleep onset (WASO) mins:	15.9 ± 16.4
Sleep onset latency (mins):	9 ± 16.6
REM latency (mins):	89.3 ± 24.9
Efficiency (%):	93.8 ± 5.3
Stage N1 sleep (mins):	30.3 ± 15.5
Stage N2 sleep (mins):	233 ± 26.4
Stage N3 sleep (mins):	77.1 ± 21.8
Total NREM sleep (mins):	340.4 ± 20.1
Stage REM sleep (mins):	101.4 ± 32.4
Stage N1 sleep (%TST):	6.9 ± 3.6
Stage N2 sleep (%TST):	52.9 ± 5.6
Stage N3 sleep (%TST):	17.6 ± 5.5
Total NREM sleep (%TST):	77.4 ± 5.5
Stage REM sleep (%TST):	22.6 ± 5.5

Differences in FC between sleep stages, within each sleep cycle and frequency band

We examined whether FC changed between sleep stages (NREM2, NREM3, and REM) within each sleep cycle (cycles one, two, and three) and each frequency band of interest (delta, theta, alpha, sigma, beta, and gamma).

Delta Band

In the first cycle of sleep, the repeated-measures ANOVA using sleep stage as a within-subject factor showed that delta-band connectivity was significantly different between NREM2, NREM3, and REM sleep within and between all network pairs (Figure 2A). Pairwise

comparisons between sleep stages showed that NREM2 connectivity was significantly higher than NREM3 and REM connectivity (Figure 2B and Supplemental Figure 2). No significant differences in connectivity were observed between NREM3 and REM sleep.

In the second cycle of sleep, there were no significant differences in connectivity between sleep stages that survived correction for multiple comparisons.

In the third sleep cycle, the main effect of sleep stages on delta-band connectivity was observed within and between almost all networks (Supplemental Figure 3A). Pairwise comparisons indicate that this effect was mainly driven by higher connectivity in NREM3 as compared to REM sleep (Supplementary Figure 3B and Supplementary Figure 4). No significant differences were found between NREM2 and NREM3 sleep.

Our results indicate that delta-band connectivity was overall higher during NREM as compared to REM sleep in cycles one and three within and between nearly all network pairs.

Theta Band

In the first sleep cycle, connectivity in the theta band differed significantly between sleep stages within and between several networks (Figure 3A). Pairwise comparisons showed this effect was primarily driven by higher connectivity during NREM2 as compared to NREM3 sleep (Figure 3B and Supplementary Figure 5). There were no differences in connectivity between NREM2 and REM.

In the second and third sleep cycles, theta-band connectivity did not differ between sleep stages.

In summary, theta-band connectivity was significantly higher in NREM2 compared to NREM3 sleep during the first cycle of the night, within and between several large-scale networks.

Alpha Band

In the first sleep cycle of the night, alpha-band connectivity did not differ significantly between sleep stages after FDR correction.

In the second sleep cycle, alpha-connectivity significantly differed between sleep stages within and between several networks (Figure 4). Pairwise comparisons show greater connectivity during NREM2 as compared to NREM3 in all network pairs (Supplementary Figure 6). During REM sleep, connectivity was higher than during NREM3 in a subset of networks (i.e., the DMN, DAN, and VIS networks; Figure 4B and Supplementary Figure 6). Connectivity did not significantly differ between NREM2 and REM.

During sleep cycle three, NREM2 connectivity was significantly higher than in NREM3 and REM between most network pairs (main effect: Supplementary Figure 7; follow up: Supplementary Figure 8).

Overall, our results show that connectivity in the alpha band was higher in NREM2 sleep compared to NREM3 in the majority of network pairs and particularly during the second and third cycles of the night. Alpha band connectivity was also greater during REM as compared to NREM3 in the second cycle of the night in a subset of network pairs, including the DAN, DMN, and VIS networks, but this effect was no longer significant in the third sleep cycle.

Sigma Band

In the first sleep cycle, sigma-band connectivity was different between sleep stages within and between several networks (Figure 5A). Pairwise comparisons indicate that connectivity was higher in NREM2 compared to both NREM3 and REM sleep (Figure 5B and Supplementary Figure 9). No significant differences were found between NREM3 and REM.

A similar pattern of results was observed in sleep cycles two (Supplementary Figure 10-11) and three (Supplementary Figure 12-13) within and between all network pairs.

In sum, sigma-band connectivity within and between nearly all large-scale networks was consistently higher in NREM2 than in other stages during the first three cycles of sleep.

Beta Band

During the first cycle of sleep, significant inter-stage differences in beta-band connectivity were observed within the default mode network, the attentional and visual networks, as well as between these networks and other networks (Figure 6A). Pairwise tests showed significantly higher FC in NREM2 as compared to NREM3 in the same networks and pairs described above and greater connectivity in REM as compared to NREM3 within and between the DMN and attentional networks (Supplementary Figure 14). No significant differences were found between NREM2 and REM sleep in this cycle.

No significant inter-stage differences were found in the second and third cycles of sleep after FDR correction.

In summary, beta-band FC within and between the DMN, visual, and attentional networks was greater in NREM2 and REM sleep as compared to NREM3 in the first cycle but not during later cycles of the night.

Gamma Band

After FDR correction, there were no significant differences in gamma-band FC between sleep stages in the first three cycles of the night.

Summary

Altogether, the results of the inter-stage analyses indicate that FC within and between almost all networks significantly decreased from NREM2 to NREM3 sleep in several frequency bands (i.e., alpha, beta, delta, sigma, and theta) and in the different sleep cycles. A similar spatially

widespread decrease in connectivity was also observed during the transition from NREM to REM in the delta and sigma frequency bands. In contrast, alpha- and beta-band connectivity increased from NREM3 to REM sleep in specific networks (i.e., the DMN and the attentional networks).

Differences in FC between sleep cycles, within each sleep stage and frequency band

We here examined whether FC changed between sleep cycles (one, two, and three) within each sleep stage (NREM2, NREM3, and REM) and each frequency band of interest (delta, theta, alpha, sigma, beta, and gamma).

NREM2

The repeated-measures ANOVA on NREM2 connectivity metrics using sleep cycle as a within-subject factor did not show any main effect of sleep cycle in any of the examined frequency bands and network pairs.

NREM3

Similar to the above, there were no significant differences in connectivity between cycles of NREM3 sleep that survived correction for multiple comparisons in any of the examined frequency bands and network pairs.

REM

The repeated-measures ANOVA examining inter-cycle changes in REM connectivity showed that gamma-band connectivity within and between several networks (excluding the visual network) was significantly different between the three sleep cycles (Figure 7A). Follow-up tests revealed that this effect was driven by significant increases in gamma-connectivity from cycle 2 to cycle 3 (Figure 7B and Supplementary Figure 15). There were no differences in connectivity between cycles 1 and 2.

Discussion:

The goal of this study was to investigate how frequency-dependent connectivity within and between large-scale resting-state networks changed across stages and cycles of overnight sleep in healthy young adults. Our results show that connectivity within and between almost all networks significantly decreased from NREM2 to NREM3 sleep in multiple frequency bands (i.e., alpha, beta, delta, sigma, and theta) and in the different sleep cycles. This breakdown in connectivity was also observed as sleep progressed from NREM to REM sleep in almost all networks in the delta and sigma frequency bands. In contrast, alpha- and beta-band connectivity increased from NREM3 to REM sleep in the DMN and the attentional networks. Interestingly, REM sleep gamma-band connectivity was particularly increased in cycle three as compared to earlier cycles during the night in all network pairs, excluding the visual network. Overall, our data show two main connectivity profiles during

sleep: (1) a pronounced overall decrease in connectivity across multiple networks and frequency bands as NREM sleep deepens and (2) frequency- and network-specific modulations of connectivity during the transition to REM sleep.

NREM2

Our results revealed that NREM2 sleep, as compared to other sleep stages, is characterized by an overall elevated level of functional connectivity in multiple frequency bands and network pairs in the different sleep cycles. Specifically, NREM2 FC was higher than during NREM3 in the alpha, beta, delta, sigma, and theta bands in the three sleep cycles (but see below for a discussion on delta connectivity). NREM2 FC was also significantly higher than REM FC in the delta and sigma bands during all cycles. Our results are consistent with previous work showing higher cortico-cortical connectivity in lighter sleep (i.e., NREM1 and NREM2; Larson-Prior et al., 2009; Spoormaker et al., 2010) compared to other sleep stages. It has been proposed that these network configurations may be related to brain plasticity processes, with increased connectivity during lighter NREM sleep being involved in the global transfer of information (Spoormaker *et al.*, 2011). Studies of dynamic functional connectivity have shown an increase in inter-network co-occurrence during NREM2; however, this was accompanied by unstable synchronization (Tarun *et al.*, 2021). Higher connectivity during NREM2 might therefore reflect increased inter-network communication that might not be fully efficient for information transfer (Kung *et al.*, 2019; Tarun *et al.*, 2021). Our data indicate that these connectivity patterns during NREM2 are widespread on both the frequency and spatial dimensions, as they were observed across multiple frequency bands and network pairs. They were also observed in all sleep cycles, which is consistent with previous literature showing steady global connectivity during NREM2 across the first three cycles of sleep in the high-delta frequency (Bouchard *et al.*, 2019). We speculate that the recurrent widespread spatio-temporal NREM2 connectivity patterns across the night might support the repeated attempt toward information transfer suggested in earlier work (Spoormaker *et al.*, 2011). Nonetheless, future research is warranted to examine the link between such large-scale network communication and brain plasticity processes during NREM2 sleep.

NREM3

We observed a consistent decrease in FC from NREM2 to NREM3 across all the examined networks and frequency bands (excluding the gamma band, and see below for a discussion of the delta band). These findings are in line with previous research showing that the descent to deep sleep is accompanied by a decrease in long-range inter-cortical FC (Horovitz *et al.*, 2009; Tagliazucchi *et al.*, 2012; Deco *et al.*, 2014), as well as a dampening of inter-regional effective connection dynamics (Massimini *et al.*, 2005), and segregation of FC into smaller modules (Boly *et al.*, 2012; Spoormaker *et al.*, 2012). Note, however, that several of these seminal studies reported a decrease in FC from wakefulness to NREM sleep (stages 2 and 3 combined, e.g., Massimini et al., 2005; Ferri et al., 2008; Boly et al., 2012), whereas the

breakdown in connectivity observed in the current study occurred between NREM2 and NREM3 sleep stages. Nevertheless, our results concur with these earlier observations of a decrease in connectivity as NREM sleep deepens. Here, we show that this decrease in connectivity is widespread in both the spatial and temporal domains.

At the network level, the reduced communication between regions of sensorimotor and executive networks is thought to support the fading of sensory awareness and disengagement of executive control during sleep (Larson-Prior *et al.*, 2009; Wu *et al.*, 2012; Daneault *et al.*, 2021). The decrease in FC between nodes of the DMN (particularly in the frontal regions) during NREM3 has been proposed to reflect the decrease in conscious awareness that characterizes this stage of sleep (Horovitz *et al.*, 2009; Sämann *et al.*, 2011; Wu *et al.*, 2012). Note, however, that DMN connectivity has also been described to be maintained throughout all stages of sleep (Koike *et al.*, 2011) or even to increase from NREM2 to NREM3 (Watanabe *et al.*, 2014). In the frequency domain, earlier studies have mainly reported greater connectivity during NREM3 as compared to wake and other sleep stages in the beta (Ferri *et al.*, 2008), alpha, and sigma (Achermann *et al.*, 2016) frequency bands. This is in contradiction with our results showing a general decrease in alpha, beta, and sigma connectivity during NREM3. While the origin of these discrepancies remains unclear, it is worth noting that the nature of the connectivity metrics extracted in these studies is different from ours (i.e., channel vs. source level; graph theory / global field synchronization vs. power envelope correlation). With respect to connectivity in the delta band, our results are in line with recent studies reporting lower connectivity (coherence measures) during NREM3 compared to other states of consciousness (i.e., wake, NREM2, and REM; Bouchard et al., 2019). Interestingly, the breakdown in connectivity observed in the delta-band was more pronounced in the first sleep cycle than later during the night, wherein delta-band NREM3 connectivity was rather elevated. These findings are consistent with research showing global increases in NREM3 delta-band connectivity across sleep cycles (Bouchard *et al.*, 2019) and suggest that the well-known breakdown in connectivity during NREM sleep is preferentially observed early during the night – at least in the delta frequency band. The breakdown in large-scale connectivity and increased modularity during NREM sleep have been proposed in earlier research to support functionally segregated information processing (Spoormaker *et al.*, 2011). Such local processing is thought to be optimal for memory consolidation as it would allow memories to be maintained in specialized networks with limited potential interfering influence from other networks (Andrade et al., 2011; Spoormaker et al., 2011; and see Niknazar et al., 2022 for slow oscillation-based long-range communication).

REM

REM connectivity analyses revealed two different spatiotemporal patterns of results. On the one hand, we report a persistence of the breakdown in connectivity observed in deep NREM sleep into REM, within and between almost all network pairs in the delta and sigma

frequency bands. In contrast, alpha- and beta-band connectivity increased significantly from NREM3 to REM sleep within the attentional and default mode networks as well as between these networks and distant networks. Our results, therefore, indicate that the modulation of connectivity profiles during the transition to REM sleep is frequency- and network-specific. We suggest that this might explain some of the discrepant findings reported in earlier studies focusing on the spatial or temporal components of connectivity separately. For example, earlier research has shown various patterns of results for DMN connectivity during REM sleep (i.e., maintenance of connectivity in core DMN seeds: Koike et al., 2011; increase in connectivity in subcomponents of the DMN: Koike et al., 2011; and decrease in DMN connectivity: Watanabe et al., 2014). Here, we show that such modulations are frequency-dependent, as we observed maintenance of delta and sigma DMN connectivity but also an increase in alpha and beta DMN connectivity; and we argue that these modulations might reflect different processes. Specifically, our data suggest that modulations in the delta and sigma bands reflect the persistence of the breakdown in connectivity described in NREM3 in all networks. This is partially supported by recent coherence analyses that show similar levels of connectivity between NREM3-REM in the delta frequency, at least in the first cycle of sleep (Bouchard *et al.*, 2019). In contrast, the increase in connectivity in the alpha and beta bands observed in the DMN and attentional networks might reflect the specific reconnection of these networks to wake-like connectivity states, as suggested in previous research (Wu *et al.*, 2012; Houldin *et al.*, 2021) and observed in various frequency bands including alpha and beta (Achermann *et al.*, 2016). Importantly, our data show that such reconnection during REM sleep occurred in frequency bands that are specifically associated with the network's intrinsic connectivity during wakefulness (i.e., alpha and beta bands for the DMN and attentional networks, respectively; Samogin et al., 2019, 2020). Altogether, our results shed light on a complex pattern of connectivity during REM sleep that is consistent with both breakdown and reconnection processes that are network- and frequency-specific.

Our cross-cycle analyses demonstrate a significant increase in gamma-band connectivity in all networks (except the visual network pairs) between the second and third cycles of sleep. While early EEG research demonstrated an uncoupling between frontal and cortical sensory processing regions in the gamma band during REM sleep (Pérez-Garci *et al.*, 2001; Corsi-Cabrera *et al.*, 2003), more recent findings indicate greater global gamma-band synchronization during REM compared to other sleep stages (Achermann *et al.*, 2016). Interestingly, animal research has consistently shown theta-gamma coupling in the neocortex during REM sleep (Scheffzük *et al.*, 2011; Brankačk *et al.*, 2012), and such coupling is thought to support the processing of information encoded during wakefulness (Bandarabadi *et al.*, 2019). Indeed, gamma-theta phase-amplitude coupling in the waking brain has been described as a crucial marker of memory formation (Lisman, 2010; Sauseng et al., 2010), and long-range gamma coupling during wake is also thought to support the integration of cognitive processes (Miltner *et al.*, 1999; Rodriguez *et al.*, 1999; Varela *et al.*, 2001). Together

with evidence that REM becomes a more prominent sleep stage later in the night (Dijk *et al.*, 1990; Aeschbach & Borbély, 1993), we speculate that the increased gamma band connectivity in large-scale networks throughout the night may reflect an increase in information processing and integration of information as REM becomes more dominant. Intriguingly, we found that gamma FC was increased within and between all network pairs examined except for the visual network. Early evidence from positron emission tomography (PET) imaging suggests that visual association areas and their projections during REM sleep may operate in a closed, interoceptive system dissociated from regions that mediate interactions with the external world (Braun *et al.*, 1998). We therefore speculate that the lack of gamma connectivity increase in the visual network and between the visual and other networks during REM might reflect this segregation. This remains, however, hypothetical.

Conclusion

In the present hdEEG study, we examined network- and frequency-specific patterns of functional connectivity across stages and cycles of overnight sleep. Our results showed that long-range connectivity within and between all the canonical networks was particularly elevated during NREM2 in all frequency bands before breaking down as sleep deepens into NREM3. We also highlighted a complex modulation of connectivity patterns during the transition to REM sleep whereby the delta and sigma bands hosted a persistence of the NREM3 connectivity breakdown in all networks, whereas a reconnection was observed in the DMN and the attentional networks in the alpha and beta bands, respectively. Altogether, these data indicate that the well-known breakdown in connectivity observed as NREM sleep deepens is a general process that is similar across all networks and frequency bands. In contrast, a more complex pattern of connectivity was observed during REM sleep which is consistent with both breakdown and reconnection processes that are network- and frequency-specific.

References:

Achermann, P., Rusterholz, T., Dürr, R., König, T., & Tarokh, L. (2016) Global field synchronization reveals rapid eye movement sleep as most synchronized brain state in the human EEG. *R Soc Open Sci*, **3**.

Adamantidis, A., Gutierrez Herrera, C., & Gent, T.C. (2019) Oscillating circuitries in the sleeping brain. *Nat Rev Neurosci*, **20**, 746–762.

Aeschbach, D. & Borbély, A.A. (1993) All-night dynamics of the human sleep EEG. *J Sleep Res*, **2**, 70–81.

Andrade, K.C., Spoormaker, V.I., Dresler, M., Wehrle, R., Holsboer, F., Samann, P.G., & Czisch, M. (2011) Sleep Spindles and Hippocampal Functional Connectivity in Human NREM Sleep. *Journal of Neuroscience*, **31**, 10331–10339.

Bandarabadi, M., Boyce, R., Herrera, C.G., Bassetti, C.L., Williams, S., Schindler, K., & Adamantidis, A. (2019) Dynamic modulation of theta-gamma coupling during rapid eye movement sleep. *Sleep*, **42**, 1–11.

Bechtold, B. (2016) Violin Plots for Matlab.

Beck, A.T. (1961) An Inventory for Measuring Depression. *Arch Gen Psychiatry*, **4**, 561.

Beck, A.T., Epstein, N., Brown, G., & Steer, R.A. (1988) An inventory for measuring clinical anxiety: Psychometric properties. *J Consult Clin Psychol*, **56**, 893–897.

Benjamini, Y. & Hochberg, Y. (1995) Controlling the False Discovery Rate: A Practical and Powerful Approach to Multiple Testing. *Journal of the Royal Statistical Society: Series B (Methodological)*, **57**, 289–300.

Biswal, B., Zerrin Yetkin, F., Haughton, V.M., & Hyde, J.S. (1995) Functional connectivity in the motor cortex of resting human brain using echo-planar mri. *Magn Reson Med*, **34**, 537–541.

Biswal, B.B., Van Kylen, J., & Hyde, J.S. (1997) Simultaneous assessment of flow and BOLD signals in resting-state functional connectivity maps. *NMR Biomed*, **10**, 165–170.

Boly, M., Perlbarg, V., Marrelec, G., Schabus, M., Laureys, S., Doyon, J., Pelegrini-Issac, M., Maquet, P., Benali, H., Pélégrini-Issac, M., Maquet, P., & Benali, H. (2012) Hierarchical clustering of brain activity during human nonrapid eye movement sleep. *Proceedings of the National Academy of Sciences*, **109**, 5856–5861.

Bouchard, M., Lina, J.-M., Gaudreault, P.-O., Dubé, J., Gosselin, N., & Carrier, J. (2019) EEG connectivity across sleep cycles and age. *Sleep*, 1–10.

Brankačk, J., Scheffzük, C., Kukushka, V.I., Vyssotski, A.L., Tort, A.B.L., & Draguhn, A. (2012) Distinct features of fast oscillations in phasic and tonic rapid eye movement sleep. *J Sleep Res*, **21**, 630–633.

Braun, A.R., Balkin, T.J., Wesensten, N.J., Gwadry, F., Carson, R.E., Varga, M., Baldwin, P., Belenky, G., & Herscovitch, P. (1998) Dissociated Pattern of Activity in Visual Cortices and Their Projections During Human Rapid Eye Movement Sleep. *Science (1979)*, **279**, 91–95.

Březinová, V. (1974) Sleep cycle content and sleep cycle duration. *Electroencephalogr Clin Neurophysiol*, **36**, 275–282.

Buysse, D.J., Reynolds, C.F., Monk, T.H., Berman, S.R., & Kupfer, D.J. (1989) The Pittsburgh sleep quality index: A new instrument for psychiatric practice and research. *Psychiatry Res*, **28**, 193–213.

Corsi-Cabrera, M., Miró, E., Del-Río-Portilla, Y., Pérez-Garci, E., Villanueva, Y., & Guevara, M.A. (2003) Rapid eye movement sleep dreaming is characterized by uncoupled EEG activity between frontal and perceptual cortical regions. *Brain Cogn*, **51**, 337–345.

Daneault, V., Orban, P., Martin, N., Dansereau, C., Godbout, J., Pouliot, P., Dickinson, P., Gosselin, N., Vandewalle, G., Maquet, P., Lina, J.M., Doyon, J., Bellec, P., & Carrier, J. (2021) Cerebral functional networks during sleep in young and older individuals. *Sci Rep*, **11**, 4905.

De Gennaro, L., Ferrara, M., & Bertini, M. (2000) Topographical distribution of spindles: Variations between and within NREM sleep cycles. *Sleep Research Online*, **3**, 155–160.

de Pasquale, F., della Penna, S., Snyder, A.Z., Lewis, C., Mantini, D., Marzetti, L., Belardinelli, P., Ciancetta, L., Pizzella, V., Romani, G.L., & Corbetta, M. (2010) Temporal dynamics of spontaneous MEG activity in brain networks. *Proceedings of the National Academy of Sciences*, **107**, 6040–6045.

de Pasquale, F., della Penna, S., Snyder, A.Z., Marzetti, L., Pizzella, V., Romani, G.L., & Corbetta, M. (2012) A Cortical Core for Dynamic Integration of Functional Networks in the Resting Human Brain. *Neuron*, **74**, 753–764.

Deco, G., Hagmann, P., Hudetz, A.G., & Tononi, G. (2014) Modeling resting-state functional networks when the cortex falls asleep: Local and global changes. *Cerebral Cortex*, **24**, 3180–3194.

Dijk, D.J., Brunner, D.P., & Borbély, A.A. (1990) Time course of EEG power density during long sleep in humans. *Am J Physiol Regul Integr Comp Physiol*, **258**.

Ellis, B.W., Johns, M.W., Lancaster, R., Raptopoulos, P., Angelopoulos, N., & Priest, R.G. (1981) The St. Mary's Hospital sleep questionnaire: A study of reliability. *Sleep*, **4**, 93–97.

Ferri, R., Rundo, F., Bruni, O., Terzano, M.G., & Stam, C.J. (2007) Small-world network organization of functional connectivity of EEG slow-wave activity during sleep. *Clinical Neurophysiology*, **118**, 449–456.

Ferri, R., Rundo, F., Bruni, O., Terzano, M.G., & Stam, C.J. (2008) The functional connectivity of different EEG bands moves towards small-world network organization during sleep. *Clinical Neurophysiology*, **119**, 2026–2036.

Fox, M.D., Corbetta, M., Snyder, A.Z., Vincent, J.L., & Raichle, M.E. (2006) Spontaneous neuronal activity distinguishes human dorsal and ventral attention systems. *Proc Natl Acad Sci U S A*, **103**, 10046–10051.

Gaudet, I., Hüsser, A., Vannasing, P., & Gallagher, A. (2020) Functional Brain Connectivity of Language Functions in Children Revealed by EEG and MEG: A Systematic Review. *Front Hum Neurosci*, **14**.

Greicius, M.D., Krasnow, B., Reiss, A.L., & Menon, V. (2003) Functional connectivity in the resting brain: A network analysis of the default mode hypothesis. *Proc Natl Acad Sci U S A*, **100**, 253–258.

Grootswagers, T., Cichy, R.M., & Carlson, T.A. (2018) Finding decodable information that can be read out in behaviour. *Neuroimage*, **179**, 252–262.

Haueisen, J., Ramon, C., Eiselt, M., Brauer, H., & Nowak, H. (1997) Influence of tissue resistivities on neuromagnetic fields and electric potentials studied with a finite element model of the head. *IEEE Trans Biomed Eng*, **44**, 727–735.

Hipp, J.F., Hawellek, D.J., Corbetta, M., Siegel, M., & Engel, A.K. (2012) Large-scale cortical correlation structure of spontaneous oscillatory activity. *Nat Neurosci*, **15**, 884–890.

Horne, J.A. & Ostberg, O. (1976) A self-assessment questionnaire to determine morningness-eveningness in human circadian rhythms. *Int J Chronobiol*, **4**, 97–110.

Horovitz, S.G., Braun, A.R., Carr, W.S., Picchioni, D., Balkin, T.J., Fukunaga, M., & Duyn, J.H. (2009) Decoupling of the brain's default mode network during deep sleep. *Proceedings of the National Academy of Sciences*, **106**, 11376–11381.

Houldin, E., Fang, Z., Ray, L.B., Owen, A.M., & Fogel, S. (2019) Toward a complete taxonomy of resting state networks across wakefulness and sleep: an assessment of spatially distinct resting state networks using independent component analysis. *Sleep*, **42**, 1–9.

Houldin, E., Fang, Z., Ray, L.B., Stojanoski, B., Owen, A.M., & Fogel, S. (2021) Reversed and increased functional connectivity in non-REM sleep suggests an altered rather than reduced state of consciousness relative to wake. *Sci Rep*, **11**, 1–15.

Johns, M.W. (1991) A new method for measuring daytime sleepiness: The Epworth sleepiness scale. *Sleep*, **14**, 540–545.

Koike, T., Kan, S., Misaki, M., & Miyauchi, S. (2011) Connectivity pattern changes in default-mode network with deep non-REM and REM sleep. *Neurosci Res*, **69**, 322–330.

Kung, Y.C., Li, C.W., Chen, S., Chen, S.C.J., Lo, C.Y.Z., Lane, T.J., Biswal, B., Wu, C.W., & Lin, C.P. (2019) Instability of brain connectivity during nonrapid eye movement sleep reflects altered properties of information integration. *Hum Brain Mapp*, **40**, 3192–3202.

Larson-Prior, L.J., Zempel, J.M., Nolan, T.S., Prior, F.W., Snyder, A.Z., Raichle, M.E., Snyder, A.Z., Larson-Prior, L.J., & Nolan, T.S. (2009) Cortical network functional connectivity in the descent to sleep. *Proc Natl Acad Sci U S A*, **106**, 4489–4494.

Le Bon, O., Lanquart, J.P., Hein, M., & Loas, G. (2019) Sleep ultradian cycling: Statistical distribution and links with other sleep variables, depression, insomnia and sleepiness—A retrospective study on 2,312 polysomnograms. *Psychiatry Res*, **279**, 140–147.

Lisman, J. (2010) Working memory: The importance of theta and gamma oscillations. *Current Biology*, **20**, R490–R492.

Liu, Q., Balsters, J.H., Baechinger, M., van der Groen, O., Wenderoth, N., & Mantini, D. (2015) Estimating a neutral reference for electroencephalographic recordings: the importance of using a high-density montage and a realistic head model. *J Neural Eng*, **12**, 056012.

Liu, Q., Farahibozorg, S., Porcaro, C., Wenderoth, N., & Mantini, D. (2017) Detecting large-scale networks in the human brain using high-density electroencephalography. *Hum Brain Mapp*, **38**, 4631–4643.

Mantini, D., Franciotti, R., Romani, G.L., & Pizzella, V. (2008) Improving MEG source localizations: An automated method for complete artifact removal based on independent component analysis. *Neuroimage*, **40**, 160–173.

Mantini, D., Perrucci, M.G., del Gratta, C., Romani, G.L., & Corbetta, M. (2007) Electrophysiological signatures of resting state networks in the human brain. *Proc Natl Acad Sci U S A*, **104**, 13170–13175.

Massimini, M., Ferrarelli, F., Huber, R., Esser, S.K., Singh, H., Tononi, G., Chokron, S., Bradford, D.C., Ajax, E.T., Halligan, P.W., Shulman, G.L., Goldberg, M.E., Kusunoki, M., Goldberg, M.E., Berger, M.F., Kuker, W., & Goodale, M.A. (2005) Breakdown of Cortical Effective Connectivity During Sleep. *Science (1979)*, **309**, 2228–2232.

Massimini, M., Ferrarelli, F., Murphy, M.J., Huber, R., Riedner, B.A., Casarotto, S., & Tononi, G. (2010) Cortical reactivity and effective connectivity during REM sleep in humans. *Cogn Neurosci*, **1**, 176–183.

Miltner, W.H.R., Braun, C., Arnold, M., Witte, H., & Taub, E. (1999) Coherence of gamma-band EEG activity as a basis for associative learning. *Nature*, **397**, 434–436.

Nikolaou, F., Orphanidou, C., Papakyriakou, P., Murphy, K., Wise, R.G., & Mitsis, G.D. (2016) Spontaneous physiological variability modulates dynamic functional connectivity in resting-state functional magnetic resonance imaging. *Philosophical Transactions of the Royal Society A: Mathematical, Physical and Engineering Sciences*, **374**.

Oldfield, R.C. (1971) The assessment and analysis of handedness: The Edinburgh inventory. *Neuropsychologia*, **9**, 97–113.

Pascual-Marqui, R.D., Lehmann, D., Koukkou, M., Kochi, K., Anderer, P., Saletu, B., Tanaka, H., Hirata, K., John, E.R., Prichep, L., Biscay-Lirio, R., & Kinoshita, T. (2011) Assessing interactions in the brain with exact low-resolution electromagnetic tomography. *Philosophical Transactions of the Royal Society A: Mathematical, Physical and Engineering Sciences*, **369**, 3768–3784.

Patanaik, A., Ong, J.L., Gooley, J.J., Ancoli-Israel, S., & Chee, M.W.L. (2018) An end-to-end framework for real-time automatic sleep stage classification. *Sleep*, **41**.

Pérez-Garci, E., Del-Rio-Portilla, Y., Guevara, M.A., Arce, C., & Corsi-Cabrera, M. (2001) Paradoxical sleep is characterized by uncoupled gamma activity between frontal and perceptual cortical regions. *Sleep*, **24**, 118–126.

Raichle, M.E., MacLeod, A.M., Snyder, A.Z., Powers, W.J., Gusnard, D.A., & Shulman, G.L. (2001) A default mode of brain function. *Proceedings of the National Academy of Sciences*, **98**, 676–682.

Rodriguez, E., George, N., Lachaux, J.-P., Martinerie, J., Renault, B., & Varela, F.J. (1999) Perception's shadow: long-distance synchronization of human brain activity. *Nature*, **397**, 430–433.

Sämann, P.G., Wehrle, R., Hoehn, D., Spoormaker, V.I., Peters, H., Tully, C., Holsboer, F., & Czisch, M. (2011) Development of the brain's default mode network from wakefulness to slow wave sleep. *Cerebral Cortex*, **21**, 2082–2093.

Samogin, J., Liu, Q., Marino, M., Wenderoth, N., & Mantini, D. (2019) Shared and connection-specific intrinsic interactions in the default mode network. *Neuroimage*, **200**, 474–481.

Samogin, J., Marino, M., Porcaro, C., Wenderoth, N., Dupont, P., Swinnen, S.P., & Mantini, D. (2020) Frequency-dependent functional connectivity in resting state networks. *Hum Brain Mapp*, hbm.25184.

Sauseng, P., Griesmayr, B., Freunberger, R., & Klimesch, W. (2010) Control mechanisms in working memory: A possible function of EEG theta oscillations. *Neurosci Biobehav Rev*, **34**, 1015–1022.

Savio, A., Fünger, S., Tahmasian, M., Rachakonda, S., Manoliu, A., Sorg, C., Grimmer, T., Calhoun, V., Drzezga, A., Riedl, V., & Yakushev, I. (2017) Resting-state networks as simultaneously measured with functional MRI and PET. *Journal of Nuclear Medicine*, **58**, 1314–1317.

Scheffzük, C., Kukushka, V.I., Vyssotski, A.L., Draguhn, A., Tort, A.B.L., & Brankačk, J. (2011) Selective coupling between theta phase and neocortical fast gamma oscillations during REM-sleep in mice. *PLoS One*, **6**, 1–9.

Spoormaker, V.I., Czisch, M., Maquet, P., & Jäncke, L. (2011) Large-scale functional brain networks in human non-rapid eye movement sleep: Insights from combined electroencephalographic/functional magnetic resonance imaging studies. *Philosophical Transactions of the Royal Society A: Mathematical, Physical and Engineering Sciences*, **369**, 3708–3729.

Spoormaker, V.I., Gleiser, P.M., & Czisch, M. (2012) Frontoparietal connectivity and hierarchical structure of the brain's functional network during sleep. *Front Neurol*, **MAY**, 1–10.

Spoormaker, V.I., Schröter, M.S., Gleiser, P.M., Andrade, K.C., Dresler, M., Wehrle, R., Sämann, P.G., & Czisch, M. (2010) Development of a large-scale functional brain network during human non-rapid eye movement sleep. *Journal of Neuroscience*, **30**, 11379–11387.

Taberna, G.A., Marino, M., Ganzetti, M., & Mantini, D. (2019) Spatial localization of EEG electrodes using 3D scanning. *J Neural Eng*, **16**, 026020.

Tagliazucchi, E., von Wegner, F., Morzelewski, A., Borisov, S., Jahnke, K., & Laufs, H. (2012) Automatic sleep staging using fMRI functional connectivity data. *Neuroimage*, **63**, 63–72.

Tarun, A., Wainstein-Andriano, D., Sterpenich, V., Bayer, L., Perogamvros, L., Solms, M., Axmacher, N., Schwartz, S., & van de Ville, D. (2021) NREM sleep stages specifically alter dynamical integration of large-scale brain networks. *iScience*, **24**, 101923.

Varela, F., Lachaux, J., Rodriguez, E., & Martinerie, J. (2001) The brainweb: Phase synchronization and large-scale integration. *Nat Rev Neurosci*, **2**, 229–239.

Waites, A.B., Stanislavsky, A., Abbott, D.F., & Jackson, G.D. (2005) Effect of prior cognitive state on resting state networks measured with functional connectivity. *Hum Brain Mapp*, **24**, 59–68.

Watanabe, T., Kan, S., Koike, T., Misaki, M., Konishi, S., Miyauchi, S., Miyahsita, Y., & Masuda, N. (2014) Network-dependent modulation of brain activity during sleep. *Neuroimage*, **98**, 1–10.

Wens, V., Bourguignon, M., Goldman, S., Marty, B., op de Beeck, M., Clumeck, C., Mary, A., Peigneux, P., van Bogaert, P., Brookes, M.J., & de Tiège, X. (2014) Inter- and intra-subject variability of neuromagnetic resting state networks. *Brain Topogr*, **27**, 620–634.

Wolters, C.H., Grasedyck, L., & Hackbusch, W. (2004) Efficient computation of lead field bases and influence matrix for the FEM-based EEG and MEG inverse problem. *Inverse Probl*, **20**, 1099–1116.

Wu, C.W., Liu, P.-Y., Tsai, P.-J., Wu, Y.-C., Hung, C.-S., Tsai, Y.-C., Cho, K.-H., Biswal, B.B., Chen, C.-J., & Lin, C.-P. (2012) Variations in Connectivity in the Sensorimotor and Default-Mode Networks During the First Nocturnal Sleep Cycle. *Brain Connect*, **2**, 177–190.

Ziegler, E., Chellappa, S.L., Gaggioni, G., Ly, J.Q.M., Vandewalle, G., André, E., Geuzaine, C., & Phillips, C. (2014) A finite-element reciprocity solution for EEG forward modeling with realistic individual head models. *Neuroimage*, **103**, 542–551.

Figure Legend

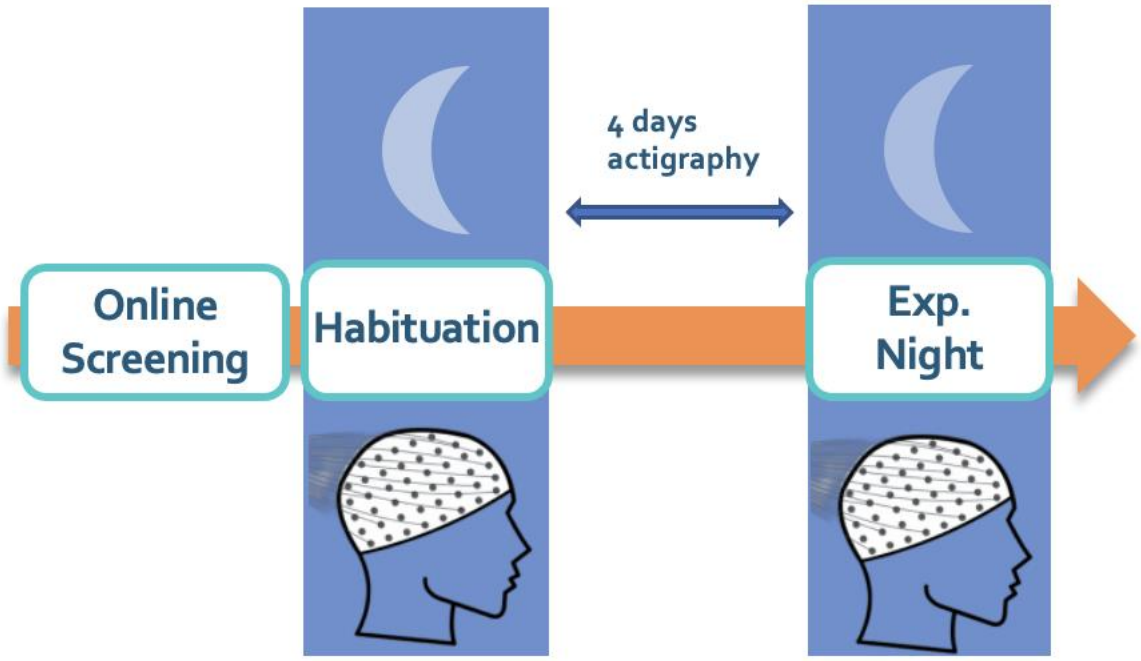

Figure 1: After completing the online screening, participants came into the lab for a habituation night with the hdEEG system. During the experimental night, participants also slept with the hdEEG system. Participants wore a wrist actigraphy device and completed a sleep diary for the four days before the experimental night to confirm adherence to a regular sleep schedule.

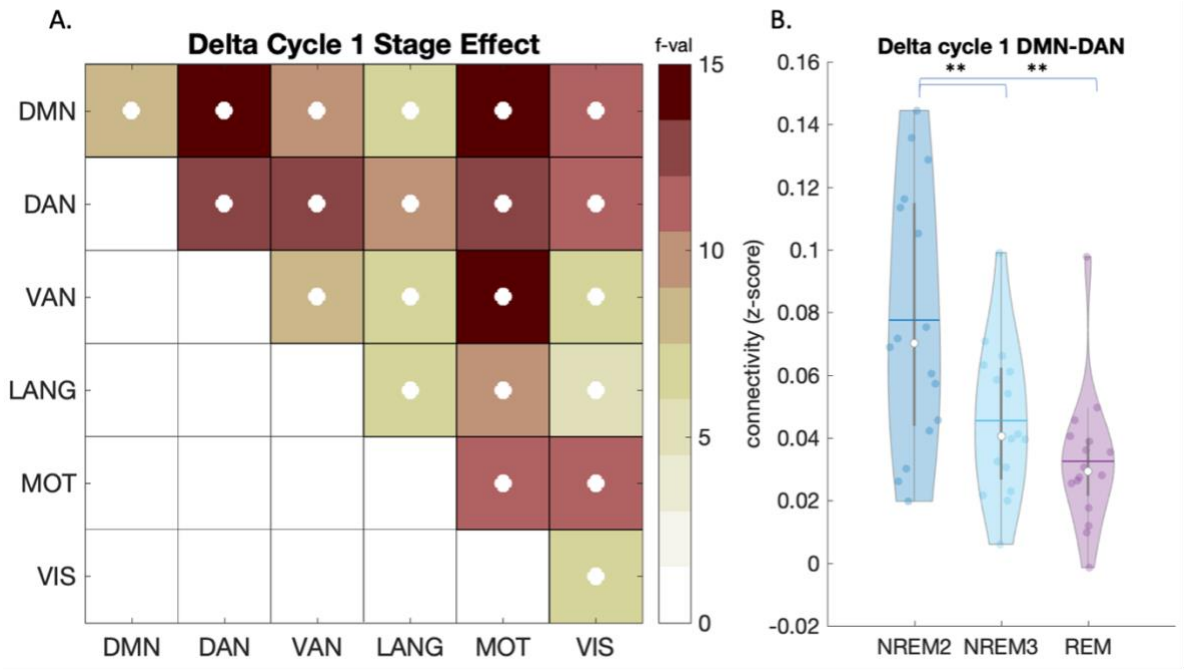

*Figure 2: A) Differences in delta-band FC between NREM2, NREM3, and REM during the first cycle of sleep (n = 16). The color scale displays ANOVA F-values. Filled circles show p < 0.05 FDR corrected across all 21 comparisons. B) rsFC between the default mode and dorsal attention networks in the delta band was significantly greater during NREM2 as compared to NREM3 and REM sleep in the first cycle of sleep. ** indicates FDR-corrected significant pairwise comparisons between sleep stages (NREM2 vs. NREM3, n = 22; NREM2 vs. REM, n = 18). Colored circles represent individual data, jittered on the x-axis. Blue horizontal lines represent means, and white circles represent medians. Violin plots were created using (Bechtold, 2016).*

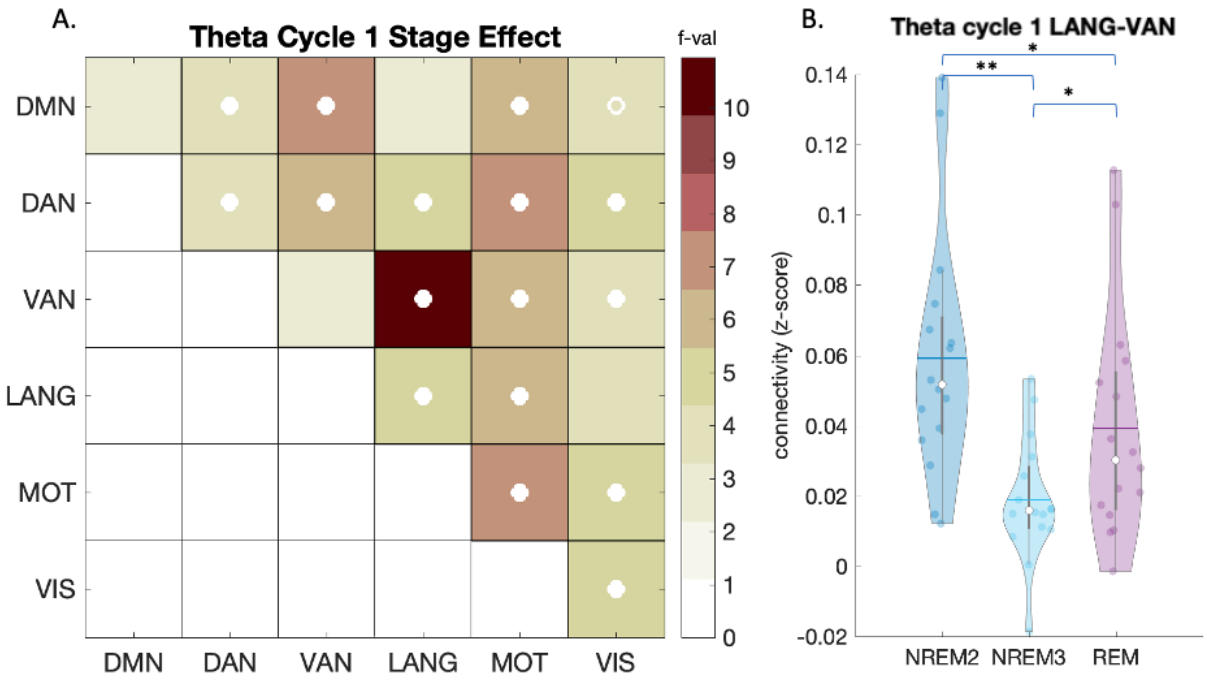

*Figure 3: A) Differences in theta-band FC between NREM2, NREM3, and REM during the first cycle of sleep (n = 16). The color scale displays ANOVA F-values. Filled circles show p < 0.05 FDR corrected across all 21 comparisons, while open circles indicate a significant correlation at p < 0.05 uncorrected. B) rsFC between the language and ventral attention networks in the theta band was greater in NREM2 compared to NREM3 in the first cycle of sleep. ** indicates FDR-corrected significant pairwise comparisons between sleep stages (NREM2 vs. NREM3, n = 22), whereas * indicates uncorrected significant pairwise comparison between sleep stages (NREM3 vs. REM, n = 16). Colored circles represent individual data, jittered on the x-axis. Blue horizontal lines represent means, and white circles represent medians.*

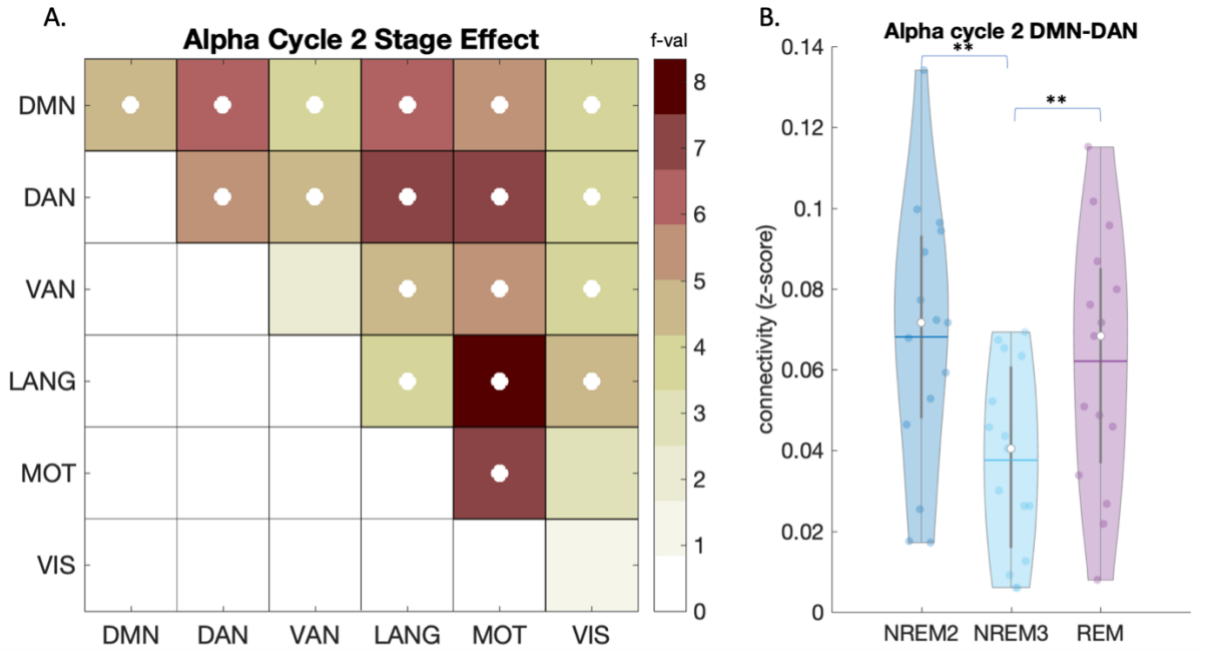

*Figure 4: A) Differences in alpha-band FC between NREM2, NREM3, and REM during the second cycle of sleep (n = 15). The color scale displays ANOVA F-values. Filled circles show p < 0.05 FDR corrected across all 21 comparisons. B) rsFC between the dorsal attention and default mode networks in the alpha band was lower in NREM3 compared to NREM2 and REM during the second cycle of sleep. ** indicates FDR-corrected significant pairwise comparisons between sleep stages (NREM2 vs. NREM3, n = 21; REM vs. NREM3, n = 18). Colored circles represent individual data, jittered on the x-axis. Blue horizontal lines represent means, and white circles represent medians.*

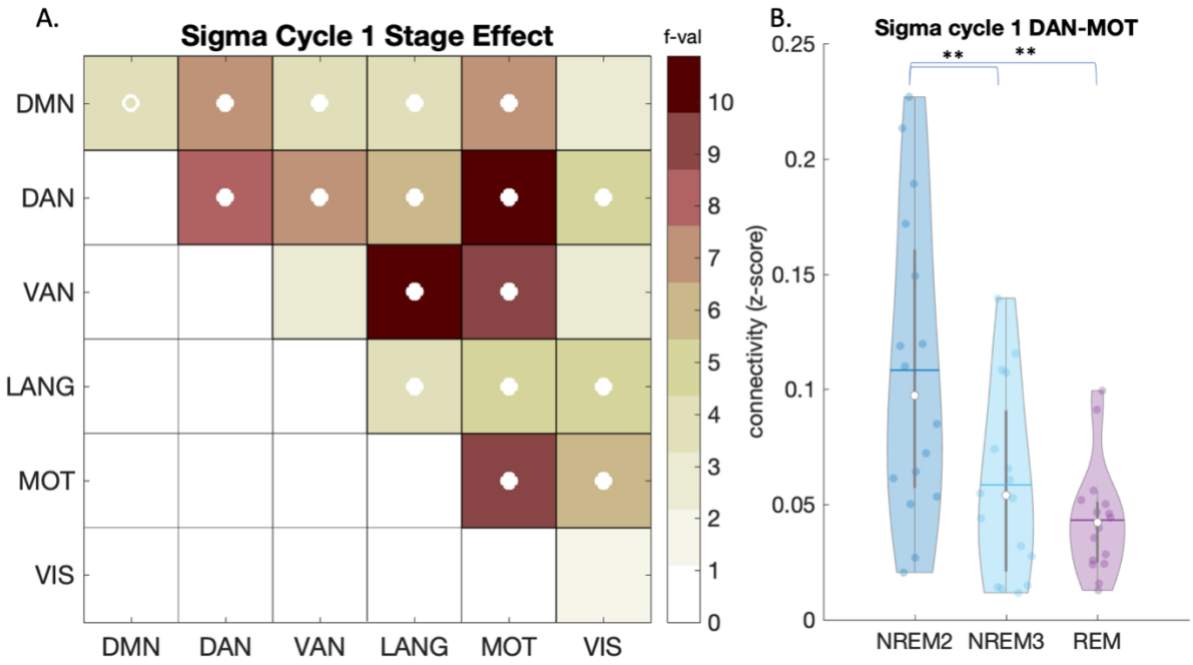

*Figure 5: A) Differences in sigma-band FC between NREM2, NREM3, and REM during the first cycle of sleep (n = 16). The color scale displays ANOVA F-values. Filled circles show p < 0.05 FDR corrected across all 21 comparisons, while open circles indicate a significant correlation at p < 0.05 uncorrected. B) rsFC between the dorsal attention and motor networks in the sigma band was higher in NREM2 compared to NREM3 and REM during the first cycle of sleep. ** indicates significant pairwise comparisons between sleep stages (NREM2 vs. REM, n = 18; NREM2 vs NREM3, n = 22). Colored circles represent individual data, jittered on the x-axis. Blue horizontal lines represent means, and white circles represent medians.*

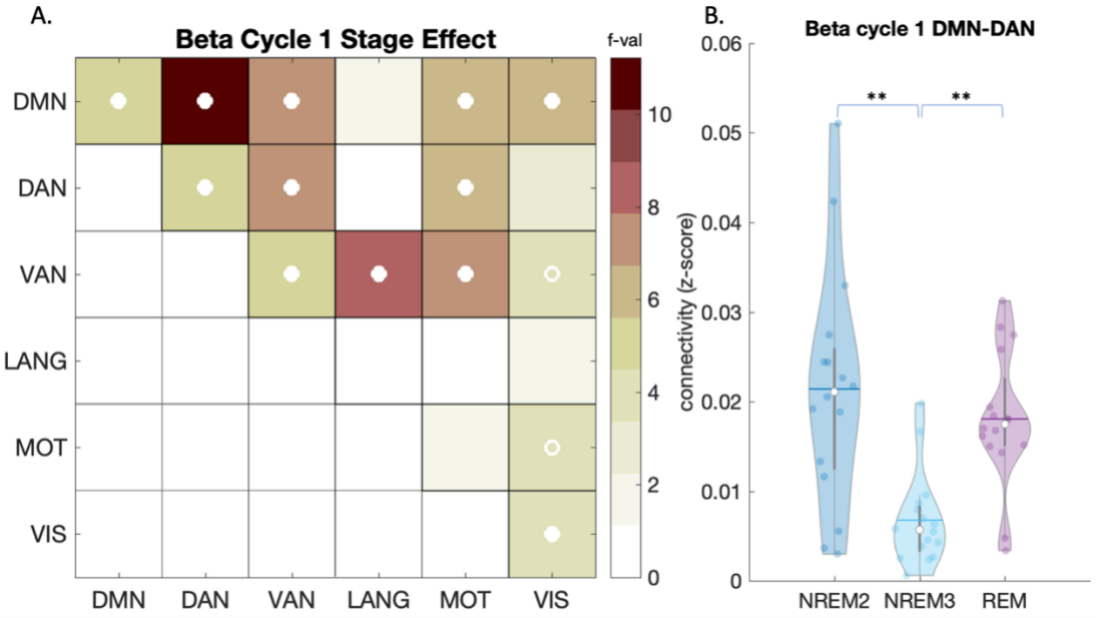

*Figure 6: A) Differences in beta-band FC between NREM2, NREM3, and REM during the first cycle of sleep (n = 16). The color scale displays ANOVA F-values. Filled circles show p < 0.05 FDR corrected across all 21 comparisons, while open circles indicate a significant correlation at p < 0.05 uncorrected. B) rsFC between the dorsal attention and default mode networks in the beta band was significantly lower during NREM3 compared to NREM2 and REM during the first cycle of sleep. ** indicates significant pairwise comparisons between sleep stages (NREM2 vs. NREM3, n = 22; NREM3 vs. REM, n = 16; NREM2 vs. REM, n = 18). Colored circles represent individual data, jittered on the x-axis. Blue horizontal lines represent means, and white circles represent medians.*

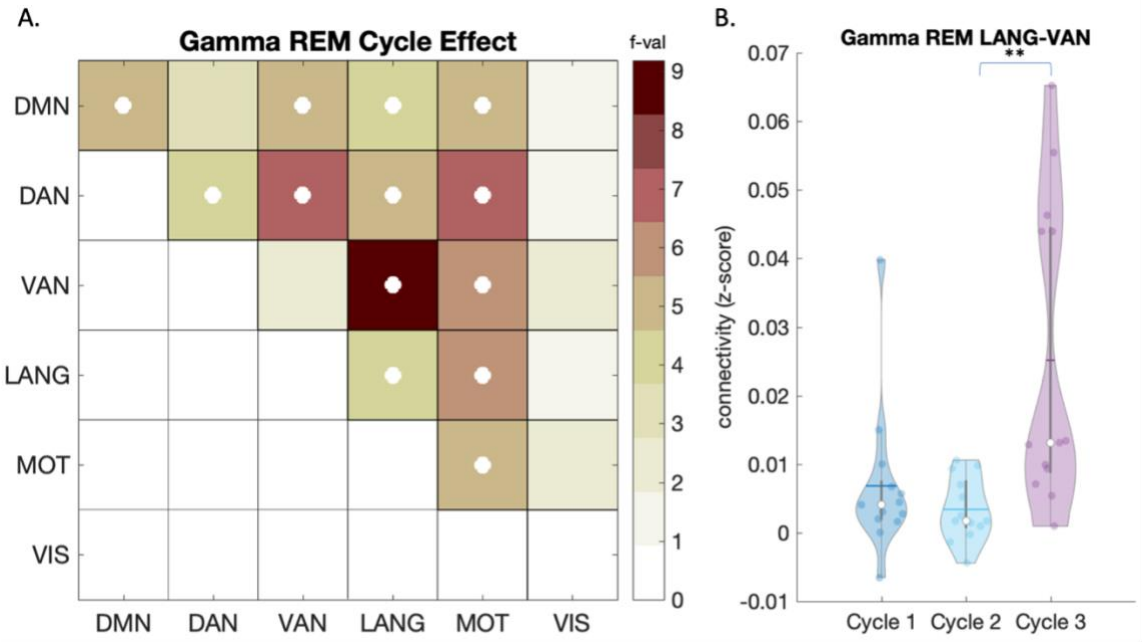

*Figure 7: A) Differences in REM sleep gamma-band FC across the first three sleep cycles (n = 13). The color scale represents ANOVA F-values. Filled circles show p < 0.05 FDR corrected across all 21 comparisons. B) rsFC between the language and ventral attention networks in the gamma band was significantly higher during the third cycle compared to the second cycle of sleep. ** indicates FDR-corrected significant pairwise comparisons between sleep cycles (cycle two vs. three, n = 16). Colored circles represent individual data, jittered on the x-axis. Blue horizontal lines represent means, and white circles represent medians.*